

RESEARCH

Open Access



Single-cell transcriptomics reveals common epithelial response patterns in human acute kidney injury

Christian Hinze^{1,2,3} , Christine Kocks⁴ , Janna Leiz^{2,3} , Nikos Karaikos⁴, Anastasiya Boltengagen⁴, Shuang Cao^{1,2,3}, Christopher Mark Skopnik^{2,5} , Jan Klocke^{2,5,6} , Jan-Hendrik Hardenberg² , Helena Stockmann² , Inka Gotthardt² , Benedikt Obermayer⁷ , Laleh Haghverdi⁴, Emanuel Wyler⁴, Markus Landthaler⁴ , Sebastian Bachmann⁸, Andreas C. Hocke^{6,9} , Victor Corman¹⁰, Jonas Busch¹¹, Wolfgang Schneider¹², Nina Himmerkus¹³ , Markus Bleich¹³ , Kai-Uwe Eckardt^{2†} , Philipp Enghard^{2,5†} , Nikolaus Rajewsky^{4†} and Kai M. Schmidt-Ott^{1,2,3*†}

Abstract

Background: Acute kidney injury (AKI) occurs frequently in critically ill patients and is associated with adverse outcomes. Cellular mechanisms underlying AKI and kidney cell responses to injury remain incompletely understood.

Methods: We performed single-nuclei transcriptomics, bulk transcriptomics, molecular imaging studies, and conventional histology on kidney tissues from 8 individuals with severe AKI (stage 2 or 3 according to Kidney Disease: Improving Global Outcomes (KDIGO) criteria). Specimens were obtained within 1–2 h after individuals had succumbed to critical illness associated with respiratory infections, with 4 of 8 individuals diagnosed with COVID-19. Control kidney tissues were obtained post-mortem or after nephrectomy from individuals without AKI.

Results: High-depth single cell-resolved gene expression data of human kidneys affected by AKI revealed enrichment of novel injury-associated cell states within the major cell types of the tubular epithelium, in particular in proximal tubules, thick ascending limbs, and distal convoluted tubules. Four distinct, hierarchically interconnected injured cell states were distinguishable and characterized by transcriptome patterns associated with oxidative stress, hypoxia, interferon response, and epithelial-to-mesenchymal transition, respectively. Transcriptome differences between individuals with AKI were driven primarily by the cell type-specific abundance of these four injury subtypes rather than by private molecular responses. AKI-associated changes in gene expression between individuals with and without COVID-19 were similar.

Conclusions: The study provides an extensive resource of the cell type-specific transcriptomic responses associated with critical illness-associated AKI in humans, highlighting recurrent disease-associated signatures and inter-individual

[†]Kai-Uwe Eckardt, Philipp Enghard, Nikolaus Rajewsky, and Kai M. Schmidt-Ott are senior authors.

*Correspondence: schmidt-ott.kai@mh-hannover.de

¹ Department of Nephrology and Hypertension, Hannover Medical School, Hannover, Germany

Full list of author information is available at the end of the article



© The Author(s) 2022. **Open Access** This article is licensed under a Creative Commons Attribution 4.0 International License, which permits use, sharing, adaptation, distribution and reproduction in any medium or format, as long as you give appropriate credit to the original author(s) and the source, provide a link to the Creative Commons licence, and indicate if changes were made. The images or other third party material in this article are included in the article's Creative Commons licence, unless indicated otherwise in a credit line to the material. If material is not included in the article's Creative Commons licence and your intended use is not permitted by statutory regulation or exceeds the permitted use, you will need to obtain permission directly from the copyright holder. To view a copy of this licence, visit <http://creativecommons.org/licenses/by/4.0/>. The Creative Commons Public Domain Dedication waiver (<http://creativecommons.org/publicdomain/zero/1.0/>) applies to the data made available in this article, unless otherwise stated in a credit line to the data.

heterogeneity. Personalized molecular disease assessment in human AKI may foster the development of tailored therapies.

Keywords: Acute kidney injury, Critical illness, Single-cell sequencing

Background

Acute kidney injury (AKI) is a frequently observed clinical syndrome, which associates with high morbidity and mortality [1–6]. More than 10% of all hospitalized individuals and more than 50% of critically ill individuals admitted to intensive care units develop AKI [2, 3, 7]. Despite its extensive clinical and economic impact, AKI therapy is largely limited to best supportive care and kidney replacement therapies (hemodialysis or hemofiltration) in patients with advanced kidney failure [8–10]. Targeted therapies preventing AKI or fostering recovery from AKI are still missing.

Numerous attempts have been made using animal models and human samples to uncover underlying mechanisms of AKI, to identify therapeutic targets and to identify disease biomarkers [11–17]. However, studies in a controlled clinical setting with cell type-specific gene expression resolution of human AKI are lacking.

Although AKI is uniformly defined by changes in serum creatinine levels and/or urinary output, previous studies suggest a vast underlying heterogeneity and complexity of AKI with an unknown number of AKI subtypes, suggesting that personalized approaches in the treatment of AKI may be needed [15, 18–20]. Most recently, the question of AKI subtypes was intensively debated when high incidence rates of AKI were observed in individuals with COVID-19 [21–24]. In particular, the question was raised whether COVID-19 entails a specific molecular subtype of AKI, through either renal viral tropism or other systemic effects [25–29].

Single-cell gene expression approaches provide powerful tools to investigate cell type-specific changes and cellular interactions and thus may help to delineate potential molecular subtypes of AKI. Recent mouse studies underlined the potential of single cell resolution for our understanding of AKI and revealed new molecular cell states associated with AKI [11, 12, 30]. Here, we present a comparative single-cell census of the human kidney in individuals with critical illness-associated AKI compared to controls without AKI.

Methods

Study cohort

For this study, we collected post mortem biopsies from eight patients with AKI and 4 control patients. AKI patients (sample names AKI 1–8) were enrolled in the study if they showed clinical criteria of severe AKI (as

defined by KDIGO criteria for AKI stage 2 or stage 3) within 5 days prior to sampling and if they developed AKI in a clinical setting of critical illness, severe respiratory infections, and systemic inflammation. All post mortem samples were collected on intensive care units of Charité-Universitätsmedizin in Berlin, Germany. The four control samples are comprised of three specimens from tumor-adjacent normal tissues (samples names Control-TN 1–3) and three post mortem biopsy specimens of one brain-dead patient from three different time points (15, 60, and 120 min after cessation of circulation, sample names Control-15 min, Control-60 min, Control-120 min) to account for post mortem effects. Samples Control-TN1-3 were collected during elective tumor nephrectomies performed at Charité-Universitätsmedizin in collaboration with the Department of Urology. The remaining control samples (post mortem biopsies) represented by samples Control-15 min, Control-60 min, and Control-120 min were collected on an intensive care unit of Charité-Universitätsmedizin.

Specimen collection

After consent of next of kin, post mortem biopsies were collected using 18G biopsy needles within 2 h from death from individuals who had died in a clinical setting of critical illness on intensive care units of Charité-Universitätsmedizin Berlin (ethics approval EA2/045/18). Control tissue from tumor-adjacent normal tissue of tumor nephrectomies was collected during tumor nephrectomies (ethics approval EA4/026/18). Kidney specimens were either stored in pre-cooled RNAlater at 4 °C for 24 h and then stored at –80 °C (for snRNA-seq) or in 4% formaldehyde (for histopathological studies and in situ hybridizations).

Single-nuclei sequencing

Kidney specimen subjected to snRNA-seq were kept at 4 °C at all times. All specimens were treated as described in detail in Leiz et al. [31].

Main steps included are as follows: Specimens were thoroughly minced in nuclear lysis buffer 1 (nuclear lysis buffer (Sigma) + Ribolock (1U/μl) + VRC (10 mM)) and homogenized using a dounce homogenizer with pastel A (Sigma D8938-1SET), filtered (100 μm), homogenized again (douncer with pastel B), filtered through a 35-μm strainer, and centrifuged (5 min, 500 g). The pellet was then resuspended in nuclear lysis buffer 2 (nuclear lysis

buffer + Ribolock (1U/ μ l)). To remove debris from the suspension, we underlayed the suspension with lysis buffer containing 10% sucrose and 1U/ μ l of Ribolock. After centrifugation (5 min, 500 g), the supernatant and debris were carefully removed. Pelleted nuclei were resuspended in PBS/0.04%BSA + Ribolock (1U/ μ l), filtered through a 20- μ m strainer and stained with DAPI.

All samples were subjected to single-nuclei sequencing following the 10 \times genomics protocol for Chromium Next GEM Single Cell 3' v3.1 chemistry targeting 10,000 nuclei. Obtained libraries were sequenced on Illumina HiSeq 4000 sequencers (paired-end). Digital expression matrices were generated using the Cellranger software version 3.0.2 with –force-cells 10,000 against a genome composed of the human HG38 genome (GRCh38 3.0.0) and the genome of Sars-CoV-2.

Single-nuclei sequencing data analysis

Initial filtering was performed by excluding nuclei with more than 5% mitochondrial reads and less than 500 detected genes. Nuclei passing this filter of all samples were then analyzed using Seurat's best practice workflow for data integration using the reciprocal PCA approach (https://satijalab.org/seurat/articles/integration_rpca.html) with default parameters. Emerging clusters were then analyzed for marker gene expression using Seurat's FindAllMarkers function and subsequently assigned to the major renal cell types. Each major cell type was then subclustered using Seurat's best practice standard workflow for data integration: (<https://satijalab.org/seurat/articles/introduction.html>). Followed by RunUMAP(seu, dims = 1:30), FindNeighbors(seu, dims = 1:30) and FindClusters(seu, resolution = 0.5) using the integrated assay. Marker genes for all emerging clusters were calculated.

During the next steps, the aim was to identify destroyed nuclei and doublets. For the destroyed nuclei, in the initial clustering, they clearly clustered away from major kidney cell types and showed a significantly reduced complexity of gene expression (nUMI, nGene) when compared to major cell types. Removal of destroyed nuclei led to a reduction of initially 121,933 nuclei to 113,137 nuclei in our dataset. Doublets could be detected by clusters in the subclusterings of the major cell types showing canonical marker genes from another major cell type (e.g., TAL marker gene expression in a PT subcluster). Also, these subclusters clearly clustered away from the subclusters of the respective major cell type. Canonical marker genes used for doublet removal were NPHS2 (Podo), LRP2 (PT), AQP1, CLCNKA (tL), SLC12A1 (TAL), SLC12A3

(DCT), CALB1 (CNT), AQP2 (CD-PC), FOXI1 (CD-IC), PECAM1 (EC), PTPRC (Leuk), and ACTA2 (IntC). Doublet removal led to a reduction of nuclei as stated in the table in Additional file 1: Fig. S1.

Destroyed and doublet cells were removed and the whole clustering process was repeated to avoid any influence of the excluded cells on the clusterings.

After the identification of major cell types (Fig. 1), all major cell types were subclustered, separately using RunPCA, FindNeighbors, and FindClusters with resolution 0.5. This resulted in the presented subclusters in Figs. 3, 4, and 6 and the corresponding supplemental figures.

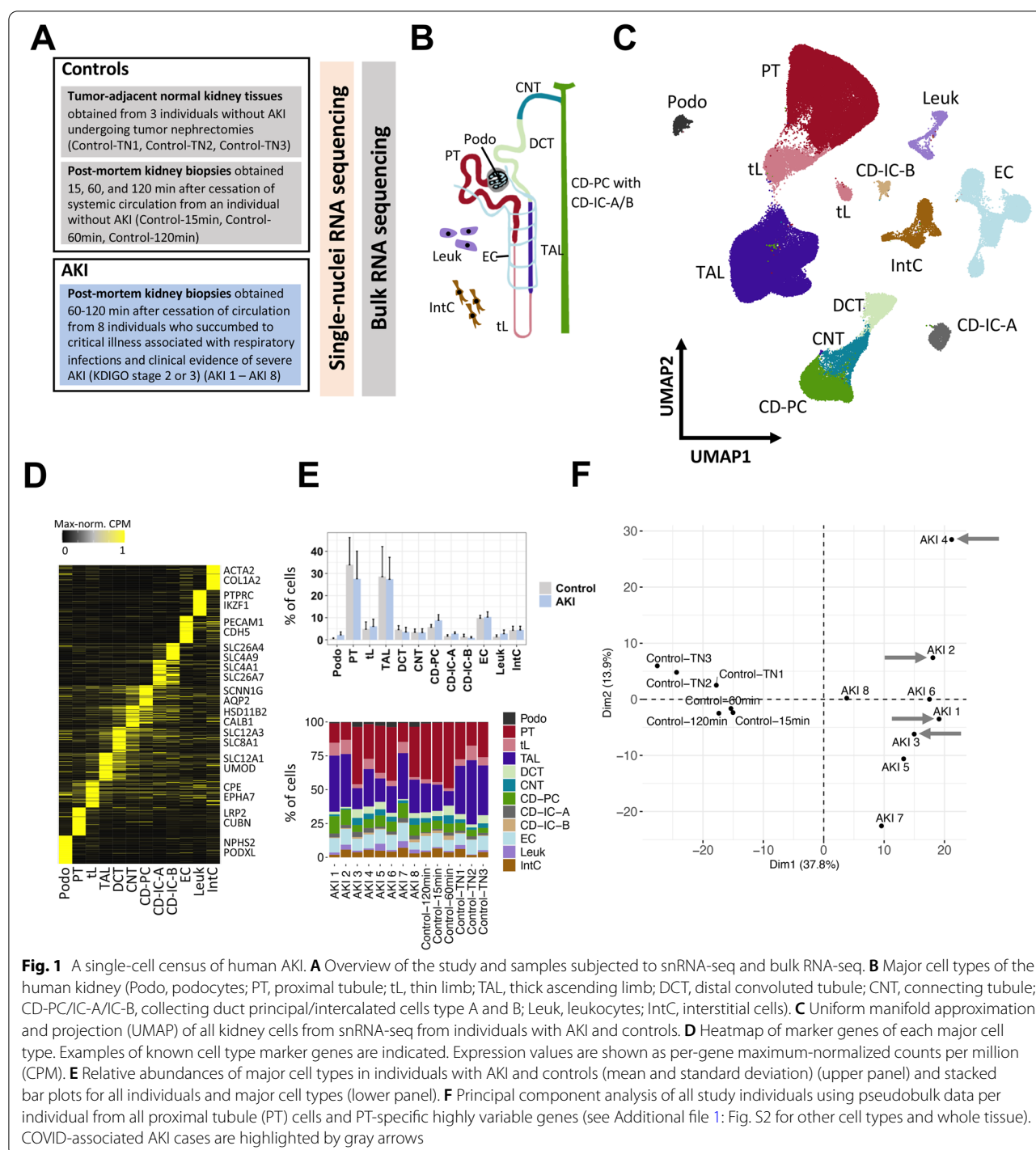
Enrichment testing for all major cell types was performed by calculating relative abundances of each generated subcluster per patient as percent of the respective major cell type. A *p*-value was computed by using a Mann–Whitney-*U* test comparing relative abundances of AKI samples versus control samples for each cluster and each major cell type. Enrichment scores were calculated by -log10 transforming the *p*-values and considered significant if *p*-value < 0.05. The three replicates from Control-PM were averaged to one value per comparison.

RNA extraction and alignment for bulk RNA sequencing

The RNeasy Micro Kit (#74,004, Qiagen, Hilden, Germany) was used to extract total RNA from kidney biopsies stored at –80 °C. For tissue disruption, frozen biopsy samples were transferred to ceramic bead-filled tubes (#KT03961-1–102.BK, Bertin Technologies, Montigny-le-Bretonneux, France) containing 700 μ l QIAazol Lysis reagent (#79,306, Qiagen) and homogenized for 2 × 20 s at 5000 rpm using a Precellys 24 tissue homogenizer (Bertin Technologies).

The lysate was incubated for 5 min at room temperature, mixed with 140 μ l chloroform, and centrifuged (4 °C, 12,000 \times g, 15 min). The supernatant was transferred to a fresh tube. Subsequent RNA purification was performed according to the “Purification of Total RNA from Animal and Human Tissues” protocol starting at step 4 (<https://www.qiagen.com/de/shop/pcr/rneasy-micro-kit/#resources>).

RNA concentration and integrity were evaluated with a NanoDrop Spectrophotometer (Thermo Scientific, Waltham, MA) and 2100 Bioanalyzer Instrument (Agilent Technologies, Santa Clara, CA). Paired-end RNA sequencing (Truseq stranded mRNA, 2 × 100 bp) was performed on a Novaseq 6000 SP flow cell. Provided FASTQ files were aligned using STAR [32] and the same genome as for the snRNA-seq data (GRCh38 3.0.0 with SARS-CoV1/2), reads were then counted using featureCounts [33] with -p -t exon -O -g gene_id -s 0.



Differential gene expression analysis

Differential gene expression analysis was performed using the DESeq2 [34] package (version 1.28.1). Input to DESeq2 were count matrices generated by adding the counts from all cells per sample and major cell type (for snRNA-seq) or the raw count matrices (for bulk

RNA-seq). For snRNA-seq, only genes expressed in 10% or 500 cells were considered. DESeq dataset was generated by:

```
dds <- DESeqDataSetFromMatrix(countData = my,
                                colData = col.data, design = ~ condition + perc.mt),
```

followed by:

```
dds <- estimateSizeFactors(dds, type = 'poscounts')
dds <- DESeq(dds)
```

"condition" was either AKI or control, my.count.data was generated for each major cell type, separately (snRNA-seq). Desired comparisons were derived by:

```
my.result = results(dds, contrast = c("condition", "Control", "AKI"))
```

Results were then filtered by demanding adjusted *p*-value < 0.001 and absolute log2 fold change larger than 1.

Pathway enrichment analysis

Differentially expressed genes were analyzed, separately, for genes up- and downregulated in AKI versus controls using the MSigDB [35, 36] web interface:

<http://www.gsea-msigdb.org/gsea/msigdb/annotate.jsp>

with the hallmark gene sets and curated gene sets (C1) from Biocarta [37], Kegg [38], Reactome [39], and WikiPathways [40].

Partition-based graph abstraction

The fully integrated assay from the Seurat object of the respective cell type was imported into scanpy [41] version 1.5.0. PCA and neighborhood graph was computed:

```
sc.tl.pca(data, use_highly_variable = False)
sc.pp.neighbors(data, n_pcs = 30)
```

Healthy subclusters (e.g., PT-S1-3) were summarized into one category (e.g., Healthy PT) to exclude the anatomical axis from this analysis. PAGA graph and diffusion pseudotime (dpt) were calculated. The root of diffusion pseudotime was defined to be in the first element of the healthy cells (e.g., first element in healthy PT). To further exclude the anatomic axis from pseudotime analysis, all dpt values for the healthy cells were set to 0. PAGA graph was then plotted with threshold 0.15 highlighting dpt. Dpt was min–max normalized for plotting.

Cross-species approach

Mouse ischemia reperfusion data was downloaded from GEO (GSE139107) [11]; metadata of PT subclustering from the original publication was kindly provided by Ben Humphreys. Multinomial classification was performed using the glmnet [42] package version 2.0–16. The training set included randomly selected cells (2/3 of cells) from injured mouse PT subclusterings. Genes used in the training were highly variable features of the mouse AKI data. Human orthologous genes were generated using

Biomart. Test data were the remaining 1/3 of mouse PT injured subclusters. Glmnet produces different models for different values of lambda which determines how hard overcomplexity of the respective model gets punished. Each so-generated model was tested on the test data and the model with the highest accuracy on the test data was determined. The so selected model was then applied to our human PT subclusters PT-New 1–4.

Validation of snRNA-seq results using independent dataset

The Kidney Precision Medicine Project recently published a preprint with multi-level omics data from kidneys of multiple disease etiologies (e.g., chronic kidney disease, acute kidney injury, control tissue) [43]. This study also included samples of patients with AKI and control samples. Hence, the cohort from this study provided an opportunity to validate our own findings of AKI-associated clusters in the setting of critical illness and systemic inflammation. For this, we downloaded snRNA-seq data from Lake et al. [43] (search criteria: Single-nucleus RNA-seq and "Aggregated Clustered Data"):

a87273b3-ec0d-4419-9253-2dc1dcf4a099_WashU-UCSD_KPMP-Biopsy_10X-R_05142021.h5Seurat
from atlas.kmp.org.

Following the information from Suppl. Table S1 of Lake et al., we were able to include five AKI cases (IDs: 30–10,034, 32–2, 33–10,005, 32–10,034, 33–10,006) and three control samples from tumor nephrectomies (IDs: 18–162, 18–142, 18–312). Unbiased clustering and marker gene calculation were performed as described for our own data. It is of note that the mentioned AKI specimens represented cases without critical illness and systemic inflammation.

RNA in situ hybridization

The RNAscope 2.5 HD reagent kit-brown (#322,300, Advanced Cell Diagnostics (ACD), Newark, CA, USA) was used to perform chromogenic in situ hybridization on formalin-fixed paraffin embedded kidney sections with probes directed against *IFITM3* (custom-ordered, ACD) and *IGFBP7* (#316,681, ACD).

The RNAscope multiplex fluorescent reagent kit v2 (#323,100, ACD) was used to perform fluorescent in situ hybridization on formalin-fixed paraffin embedded kidney sections with probes directed against *ALDOB* (#422,061-C3, ACD), *LRP2* (#532,391 custom-ordered in C3 channel, ACD), *MET* (#431,021-C3, ACD), *MYO5B* (#825,871, ACD), *NQO1* (#555,671-C2, ACD), *SERPINA1* (#435,441-C2, ACD), *SLC2A1* (#423,141-C2, ACD), *SLC12A1* (#577,391, ACD), and *VCAM1* (#440,371, ACD).

Kidney slices were fixed in 4% formaldehyde embedded in paraffin by the Department of Pathology of Charité-Universitätsmedizin Berlin. Paraffin-embedded kidney slices were cut into 5- μ m sections, plated on Superfrost Plus slides, air-dried overnight, baked for 1 h at 60 °C, cooled for 30 min, dewaxed, and air-dried again.

For chromogenic assays, subsequent pretreatment and RNAscope assay procedures for all probes were performed according to the “Formalin-Fixed Paraffin-Embedded (FFPE) Sample Preparation and Pretreatment” and “RNAscope 2.5 HD Detection Reagent BROWN” user manuals (ACD documents #322,452 and #322,310) as recommended by the manufacturer. Sections were counterstained with hematoxylin before dehydrating and applying coverslips using a xylene-based mounting medium. Images of the hybridized sections were captured on a Leica DM2000 LED bright field microscope.

For fluorescent assays, pretreatment and RNAscope assay procedures for all probes were performed according to the “RNAscope Multiplex Fluorescent Reagent Kit v2” user manual (ACD document #323,100) as recommended by the manufacturer. Sections were mounted with Dako Fluorescence Mounting Medium (#S3023, Dako, Carpinteria, CA, USA). Images were captured on a Zeiss Axio Imager 2 LSM 800 confocal scanning microscope.

Results

Single-nuclei RNA sequencing from human kidney samples enables the investigation of cell type-specific gene expression changes in acute kidney injury

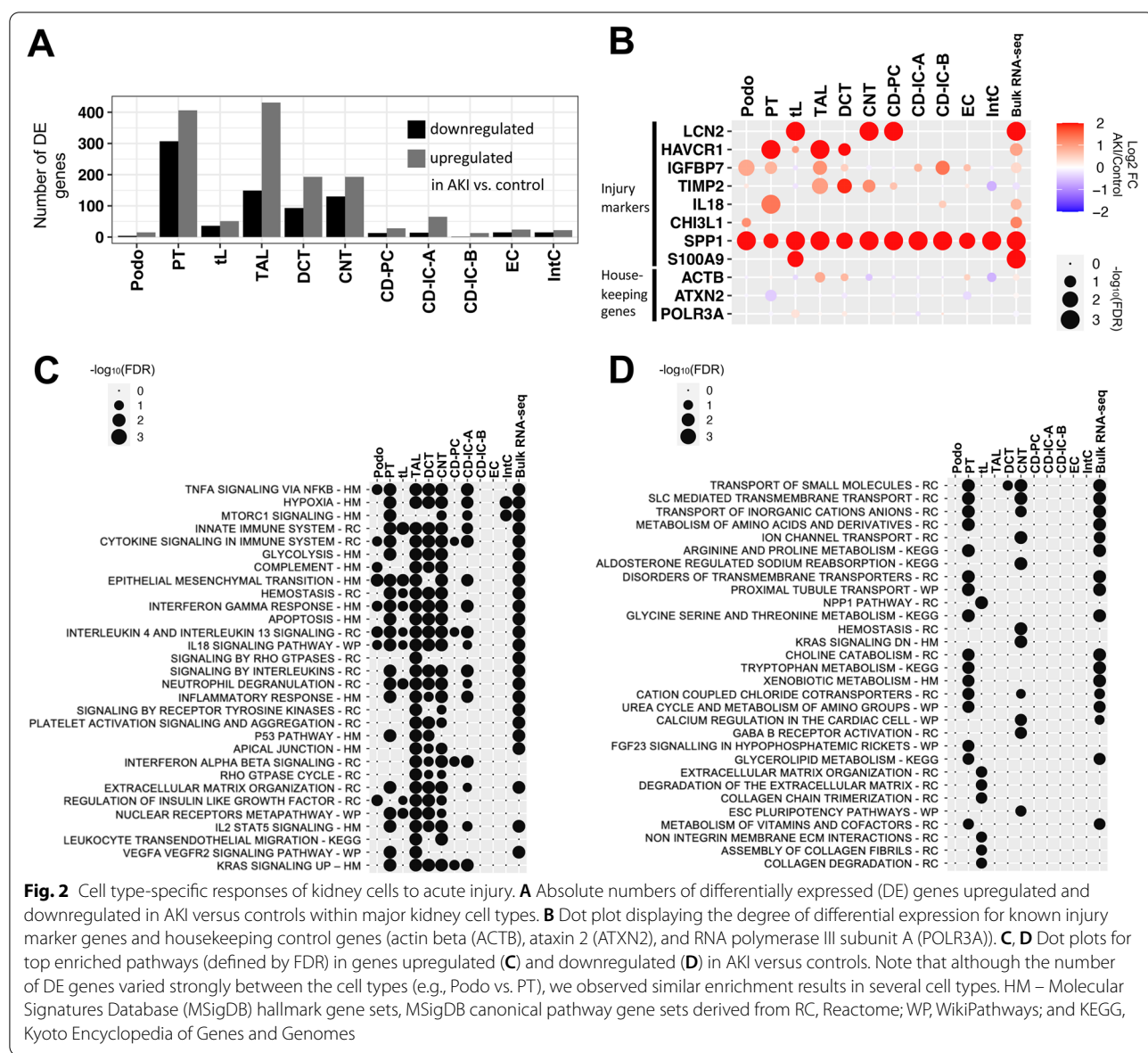
To access cellular responses in AKI, we conducted a single-cell transcriptome census of human AKI utilizing single-nuclei RNA sequencing (snRNA-seq) of kidney samples from individuals with AKI and control individuals without AKI (Fig. 1A, Additional file 1: Fig. S1). Kidney samples from individuals with AKI who succumbed to critical illness were obtained within 1–2 h post-mortem with consent of next of kin. All AKI individuals ($n=8$, AKI_{1–8}) had developed clinical criteria of severe AKI (as defined by KDIGO criteria for AKI stage 2 or stage 3) within 5 days prior to sampling. All individuals had developed AKI in a clinical setting of critical illness, severe respiratory infections, and systemic inflammation, including four cases of COVID-19-associated AKI (Additional file 2: Table S1). To control for baseline characteristics inherent to human kidneys obtained under clinical conditions and to quantitate the extent of post-mortem effects on gene expression, we used control kidney samples. They included normal kidney tissue collected during tumor nephrectomies ($n=3$; Control_{TN1-TN3}; for clinical parameters of all individuals see Additional file 2: Table S1). In addition, we obtained post-mortem kidney

tissue at three different time points (15 min, 60 min, 120 min) after the cessation of circulation (Control_{15 min; 60 min; 120 min}) from a brain-dead individual without clinical evidence of AKI.

Single-nuclei RNA-seq of all samples resulted in 106,971 sequenced nuclei with a median of 2139 detected genes and 4008 unique transcripts per nucleus (Additional file 1: Fig. S1). Joint unbiased clustering and cell type identification with known marker genes allowed the identification of the expected major kidney cell types (Fig. 1B–D). There were no overt differences in major cell type abundances between AKI and controls (Fig. 1E). Principal component analysis (PCA) indicated that the presence of AKI (versus absence of clinical AKI) was the main driver of cell type-specific and global gene expression differences between the samples (Fig. 1F, Additional file 1: Fig. S2). In contrast, PCA did not identify a major impact of the sampling method (tumor versus post-mortem biopsy), the sampling time after cessation of circulation (15 min, 60 min or 120 min), or the presence of COVID-19-associated AKI (versus AKI associated with other respiratory infections) on global or cell-type-specific gene expression (Fig. 1F, Additional file 1: Fig S2). Interestingly, we observed heterogeneity of kidney cell gene expression between different individuals with AKI (Fig. 1F).

Kidney tubular epithelial cells from different parts of the nephron show strong gene expression responses to AKI

Kidney ischemia–reperfusion injury in mice, the most frequently applied experimental model of human AKI, results in a predominant injury of cells of the proximal tubule (PT), the most abundant cell type of the kidney. Therefore, many previous studies focused on this cell type [13, 14]. However, in humans, there is considerable uncertainty regarding the impact of AKI on molecular states of different kidney cell types [44]. To assess the cell type-specific response to AKI systematically, we performed differential gene expression analysis within the major kidney cell types comparing AKI to control kidneys using DESeq2 [34] (see Additional file 3: Table S2 for a full list of differentially expressed genes per cell type). Profound transcriptomic responses to AKI were observed in kidney tubule cells of the PT, the thick ascending limb of the loop of Henle (TAL), the distal convoluted tubule (DCT), and connecting tubules (CNT), cell types that reside predominantly in the cortex and outer medulla of the kidney, regions that are known to be particular susceptible to ischemic or hypoxic injury [13–15, 45] (Fig. 2A). In contrast, less pronounced transcriptomic responses to AKI were observed in thin limbs (tL), collecting duct principal cells (CD-PCs) and



collecting duct intercalated cells (CD-ICs), consistent with the predominant localization of these cell types in the inner medulla of the kidney, which is adapted to a low oxygen environment, has lower energy expenditure, and is less susceptible to hypoxia or ischemia when compared to more cortical regions [45]. Podocytes, endothelial cells and interstitial cells also displayed less pronounced transcriptomic responses in AKI.

Among differentially expressed genes were known markers of renal cell stress, which encode proteins that have been proposed as kidney injury markers, such as neutrophil gelatinase-associated lipocalin/lipocalin 2 (LCN2), kidney injury molecule 1 (HAVCR1), and insulin-like growth factor binding protein 7 (IGFBP7) [46].

Importantly, our data provided the opportunity to identify the major cellular sources where these transcripts were synthesized in response to injury. For instance, consistent with previous reports on mouse and human AKI, LCN2 was primarily upregulated in CNT and CD-PC [12, 47], while HAVCR1 was primarily upregulated in PT [12, 48] although we also observed unexpected differential expression in TAL and DCT (Fig. 2B). Secreted phosphoprotein 1 (SPP1), encoding for the secreted glycoprotein osteopontin, was found to be upregulated in virtually all non-leukocyte kidney cell types. This was strongly reminiscent of the situation in mouse AKI, where osteopontin upregulation was similarly observed in multiple kidney cell types [12], and where osteopontin

inhibition attenuated renal injury [49], suggesting a conserved, targetable AKI pathway. IGFBP7 protein was previously found to be primarily of PT origin in diseased human kidneys [50]. Consistently, we found an upregulation of IGFBP7 mRNA in PT cells (Fig. 2B). However, we also found IGFBP7 to be upregulated in podocytes and TALs (Fig. 2B), findings which we were able to validate by IGFBP7 *in situ* hybridization (Additional file 1: Fig. S3). We also observed a strong interferon gamma response in several cell types in AKI (Fig. 2C). We could validate this finding by IFITM3 *in situ* hybridization (Additional file 1: Fig. S3). This indicates that our single-cell transcriptome database is consistent with prior knowledge and provides an opportunity to uncover novel information regarding the cellular origin of AKI-associated transcripts.

Pathway analyses of differentially expressed genes indicated that a proportion of genes upregulated in AKI were associated with inflammatory response-associated pathways (tumor necrosis factor alpha, interferon gamma, and interleukin signaling), hypoxia response, and epithelial to mesenchymal transition (EMT, Fig. 2C, Additional file 4: Table S3). Importantly, our analyses indicated that most functional pathways were upregulated simultaneously in multiple kidney tubule cell types suggesting common AKI response patterns across the nephron. Several studies have indicated an AKI-associated metabolic shift in tubular epithelia and a downregulation of genes associated with tubular transport processes [45, 51]. Consistently, we observed that genes downregulated in AKI were mostly related to molecule transport and metabolism (Fig. 2D).

Since our cohort included four individuals with COVID-19-associated AKI, we compared their kidney cell type-specific gene expression with that of individuals with non-COVID-19 respiratory infection-associated AKI. Only few differentially expressed genes were identified applying the same cut-off values for fold change and adjusted *p*-value as for the comparison between AKI and control samples (Additional file 1: Fig. S4). This suggests that the major transcriptomic responses of kidney cells in COVID-19 were not substantially different from those in other forms of AKI (see Additional file 5: Table S4 for the respective gene lists). Interestingly, a relaxation of the criteria for differential expression (adjusted *p*-value < 0.05) identified the highest number of potential gene expression differences between COVID AKI and non-COVID AKI in the DCT. This is in contrast to recent publications which report the strongest gene expression responses to COVID-19 in podocytes and PTs [52, 53] (see Additional file 1: Fig. S4, Additional file 5: Table S4 and Additional file 6: Table S5).

Importantly, the genes and pathways that were differentially regulated in AKI versus control according to

single nuclei sequencing data displayed concordant regulation in bulk mRNA sequencing from separate kidney samples of the same patients, providing additional validation (Fig. 2B, C, D).

Profound effects of AKI on kidney cell state abundance

To achieve a more fine-grained analysis of cellular subclasses, we performed subclusterings of the major kidney cell types. Thereby, we were able to derive 74 kidney cell populations based on their transcriptomes, which included known cellular subtypes of kidney cells (e.g., S1, S2, and S3 segments of the PT) and additional novel cell populations (designated as “New” cell populations, Fig. 3A, Additional file 1: Fig. S5-8, Additional file 7: Table S6). These “New” cell populations were still attributable to major kidney cell types based on their transcriptomes (Fig. 1C), but they were not characteristic of the known anatomic sub cell types, suggesting that they represent injury-related cell states.

We analyzed, which of the identified cell subpopulations differed in abundance in individuals with AKI, yielding depleted and enriched subpopulations (Fig. 3B). Profound depletion in AKI was observed within cells of the PT (in particular those representing the S3 segment), consistent with its known susceptibility to injury and its tendency to undergo dedifferentiation in AKI [11, 13, 14, 54]. Unexpectedly, in addition to PT, differentiated medullary TAL, DCT, and CNT cells were also substantially depleted in AKI. Inversely, profound enrichment in AKI was observed of the “New” cell subpopulations associated with these same cell types, indicating that PT, TAL, DCT, and CNT displayed the most profound responses to AKI and confirming the notion that “New” subpopulations represent injury-associated cell states (Fig. 3B). “New” subpopulations within cells of collecting duct (CD-PC, CD-IC-A, CD-IC-B), ascending and descending thin limbs (ATL, DTL) were also enriched in AKI, although they represented only small subpopulations (Fig. 3B), suggesting that these cell types are less susceptible or reside in less susceptible regions of the kidney. Non-epithelial cell types of the kidney, such as endothelial cells, interstitial cells, and leukocytes displayed no enrichment or depletion in AKI, with the exception of one subtype of endothelial cells (EC-New 1), which was enriched in AKI and showed a transcriptional profile resembling endothelia of descending vasa recta (Fig. 3C–F; Additional file 1: Fig. S5).

Analyses of AKI-induced cell states suggest four distinct injury response patterns

We next conducted further analyses to characterize the “New” cell subpopulations detected within the tubular epithelial compartment of the kidney. Quantification of the four “New” cell clusters associated with the PT

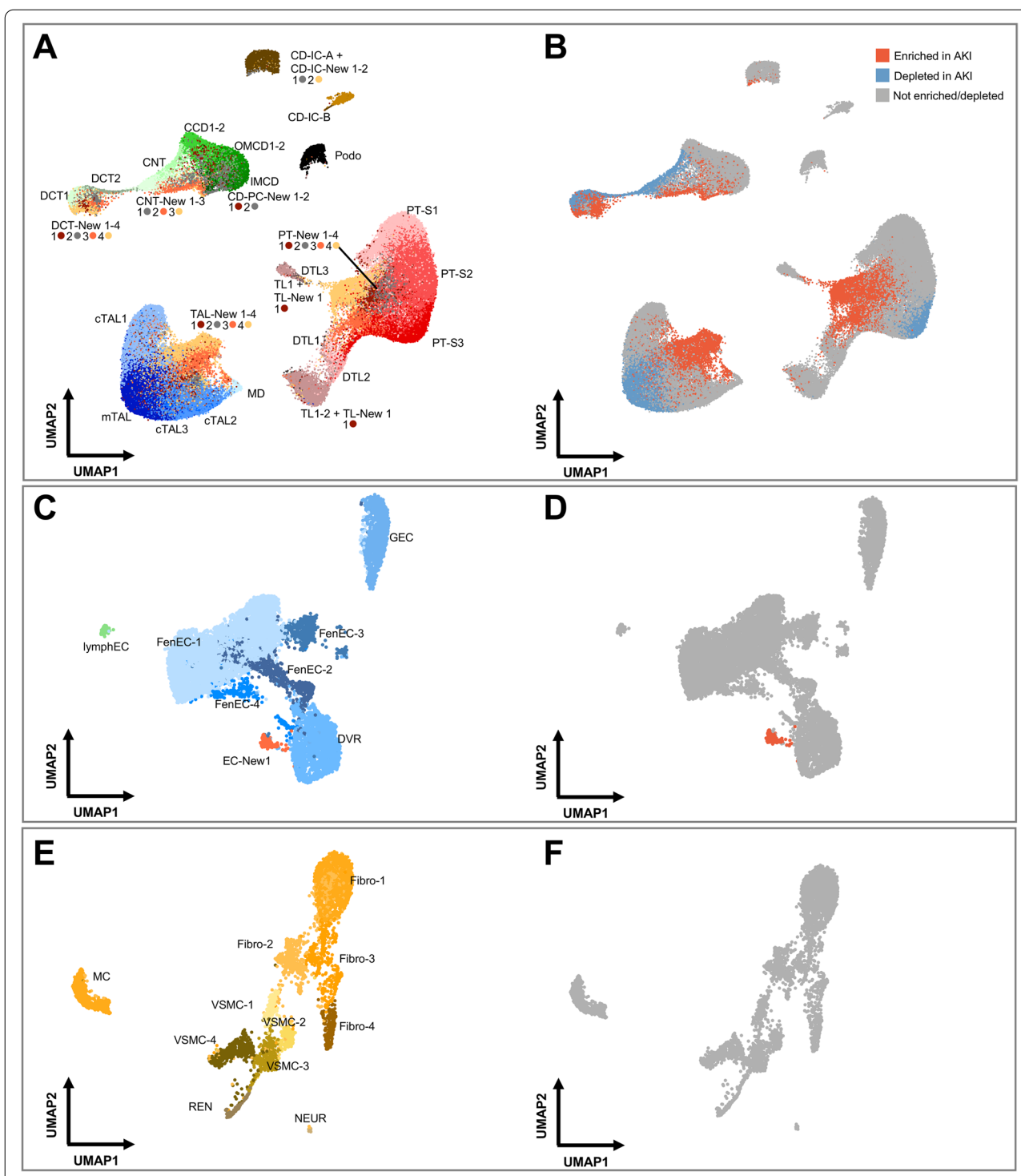
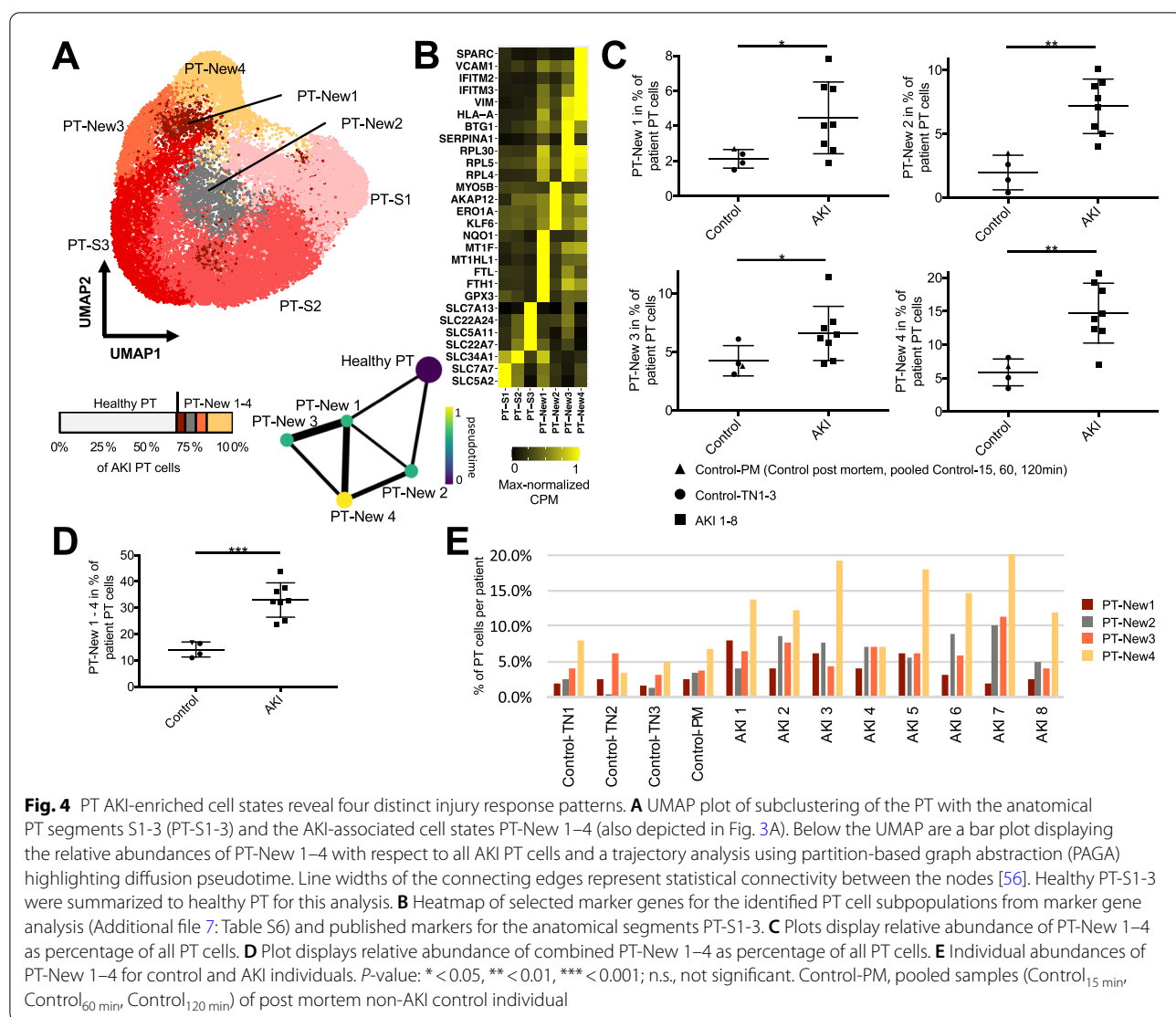


Fig. 3 AKI leads to depletion of differentiated cell states and enrichment of “New” cell states within the kidney epithelium. **A, B** UMAP plot of subclustered kidney tubular epithelial cells (**A**) and their enrichment or depletion in AKI based on statistical testing of relative abundances within the respective major cell type (**B**) (see the “Methods” section for details). In **A**, cellular subtypes of the kidney tubule are annotated as indicated. To enhance visibility, color code is indicated below the respective labeling. In **B**, the same UMAP plot as in **A** is color-coded based on enrichment (red) or depletion (blue) in AKI individuals. **C, D** Analogous plots for subclustering of endothelial cells (ECs). Please note the emergence of one AKI-associated subcluster, EC-New 1. **E, F** Analogous plots for subclusterings of interstitial cells. PT-S1-3, PT S1-3 segments; c/mTAL, cortical/medullary TAL; TL, DTL, thin limb and descending thin limb; CCD, OMCD, IMCD, cortical/outer and inner medullary collecting duct principal cell; lymphEC, lymphatic EC; GEC, glomerular EC; FenEC 1–4, fenestrated endothelial cell types; DVR, descending vasa recta; MC, mesangial cells; VSMC, vascular smooth muscle cells; REN, renin-transcribing cells; Fibro, fibroblasts; NEUR, neuronal cells



(PT-New 1–4) indicated that almost one third (31.8%) of PT cells in AKI samples belonged to these clusters (Fig. 4A). We next identified marker genes for PT-New 1–4 (Fig. 4B) and performed pathway analysis [55]. Enriched gene sets included oxidative stress signaling and the nuclear transcription factor erythroid 2-related factor 2 (NRF2) pathway (PT-New 1), the hypoxia response pathway (PT-New 2), the interferon gamma response, and genes encoding for ribosomal proteins (PT-New 3) as well as genes associated with epithelial-mesenchymal transition (EMT) (PT-New 4) (Fig. 4B, see <https://www.gsea-msigdb.org>). Hallmark and canonical pathways, for pathway definitions, additional file 7: Table S6). Nevertheless, PT-New 1–4 showed some overlap and trajectory analysis using partition-based graph abstraction (PAGA) [56] suggested hierarchical relationships between healthy PT cells and cells representing PT-New 1–4, with

PT-New 4 displaying the most distant gene expression signature from healthy PT.

We compared PT-New 1–4 to previously identified PT-derived injured cell states in mouse renal ischemia-reperfusion injury, designated as “injured PT S1/S2 cells,” “injured PT S3 cells,” “severe injured PT cells,” and “failed repair” cells [11]. We trained a multinomial model using marker genes of these clusters using a cross-species mouse/human comparative approach (see methods), which indicated that PT-New 1 (oxidative stress) showed similarity to injured mouse S1/2 cells, whereas PT-New 2 (hypoxia) resembled injured S3 cells (Additional file 1: Fig. S9). PT-New 3 and PT-New 4 most closely resembled “failed repair” PT cells in mice (Additional file 1: Fig. S9). Cells from PT-New 3 and PT-New 4 expressed the EMT marker VIM. PT-New 4 cells were additionally marked by VCAM1, a marker that has previously

been associated with the “failed repair” state of injured PT cells [57]. PT-New 1, PT-New 3, and PT-New 4 also showed high expression of interferon target genes (e.g., IFITM2, IFITM3) and human leukocyte antigen HLA-A, which is consistent with the association of injured PT cells with immune responses and inflammation [57]. Together, these observations suggest that “New” cell populations represent four distinct but hierarchically connected injured PT cell states.

The individual abundances of PT-New 1–4 and the combined abundances of PT-New 1–4 were significantly increased in the AKI samples (Fig. 4C, D). Importantly, the distribution of PT-New 1–4 among individuals with AKI displayed marked heterogeneity (Fig. 4C, E). For instance, the relative abundance of PT-New 4 (EMT/ “failed repair”) varied by a factor of three among samples from different individuals with AKI (compare PT-New 4 between AKI 4 and AKI 7 in Fig. 4E). The combined injury-associated PT clusters (PT-New 1–4) made up between 20 and 45% of all proximal tubule cells in individuals with AKI (Fig. 4C). Together these observations highlight the presence of recurrent AKI-associated cell states, but they also indicate substantial inter-individual heterogeneity.

We next aimed to validate all “New” PT-associated cell states in injured kidney tissues using multi-channel RNAscope *in situ* hybridizations. Using kidney tissue sections from AKI and control patients, we performed co-staining for LDL receptor-related protein 2 (LRP2), a transcript encoding a canonical proximal tubule marker, and four PT-New 1–4 marker transcripts. These marker transcripts were selected based on their strong and specific overexpression in either of the PT-New clusters (PT-New 1–4), and by their previously reported association with functional gene expression signatures of oxidative stress (PT-New 1, marker gene: NAPDH dehydrogenase quinone 1, NQO1), hypoxia (PT-New 2, marker gene: myosin-Vb, MYO5B), inflammation response (PT-New 3, marker gene: serpin family A member 1, SERPINA1), and EMT (PT-New 4, marker gene: vascular cell adhesion molecule 1, VCAM1) [58–61] (Fig. 5A–D). As predicted, cells representing these four cell states were detectable as subsets of cells within proximal tubules. They were highly specific to AKI patients with little or no representation in kidneys of control (non-AKI) individuals (Fig. 5A–D).

PT-New 1–4 cells were distinct from each other and were mostly interspersed among other proximal tubule cells, but sometimes occurred as local clusters (e. g. PT-New 3 and PT-New 4, Fig. 5C).

The abundance of injury response patterns varies among cell types of the kidney tubule

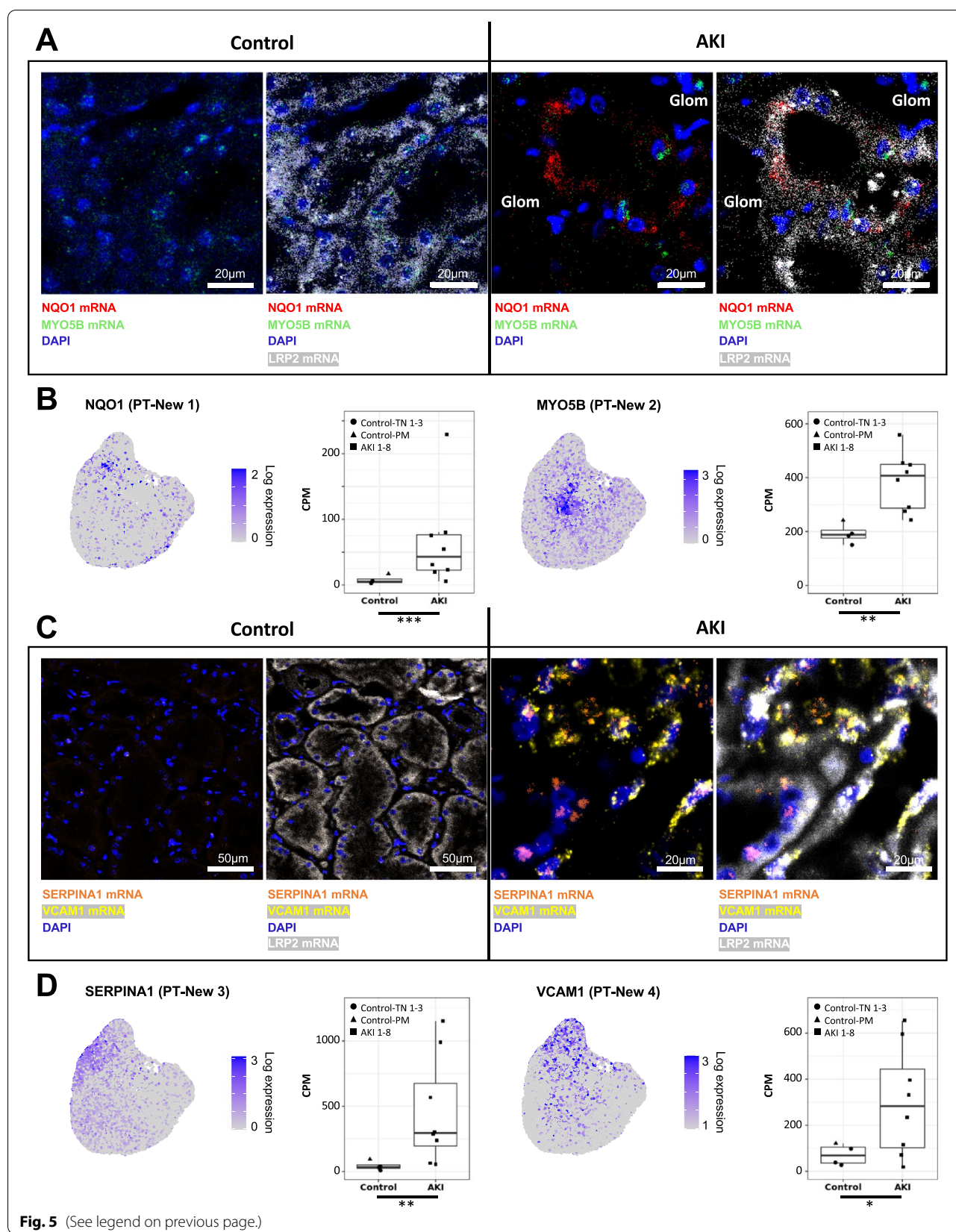
We next turned to other kidney epithelial cell types and their response to injury. We compared AKI-enriched “New” cell states in tL, TAL, DCT, CNT, CD-PC, and CD-IC to those in PT (Fig. 6A–D, Additional file 1: Fig. S10–12). Remarkably, the transcriptomic responses of the different tubular epithelial cell types to AKI displayed a marked overlap. For instance, “New” cell populations residing in TAL (TAL-New 1–4) and DCT (DCT-New 1–4) displayed four injured cell states with marker genes and functional pathways similar to PT-New 1–4 (Additional file 8: Table S7, Additional file 1: Fig. S13). This suggests conserved injury responses across different kidney cell types. To assess potential transcriptional regulation within the “New” cell populations, we performed enrichment analysis using the ChIP enrichment analysis dataset [62] with Enrichr [55] (Additional file 9: Table S8). Among top enriched transcription factors were NRF2 (New 1), hypoxia inducible factor 1 subunit alpha (New 2), MYC (New 3), and Jun proto-oncogene (New 4).

The percentage of cells displaying AKI-associated “New” cell states varied markedly among major cell types of the kidney: 31.8% of PT cells, 36.4% of TAL cells, 59.6% of DCT cells, 43.5% of CNT cells, 2.1% of tL cells, 19.1% of CD-PCs, and 5.7% of CD-ICs (Figs. 4E and 6E, Additional file 1: Fig. S10–12).

We could further validate our findings using an independent snRNA-seq dataset from kidneys of patients with non-critical illness-associated forms of AKI [43] (Additional file 1: Fig. S14). Interestingly, cells representing PT-New 1, PT-New 2, PT-New 4, TAL-New 1, TAL-New 2, and TAL-New 4 were clearly detectable within these AKI kidneys, whereas the inflammatory clusters (PT-New 3 and TAL-New 3) and interferon signatures were absent. This suggests that the “New 3” cell states

(See figure on next page.)

Fig. 5 Multi-channel *in situ* hybridizations confirm the presence of the four “New” cell states in PTs. **A** *In situ* hybridizations for oxidative stress-related gene NQO1 (marker gene for PT-New 1), hypoxia-associated gene MYO5B (marker gene for PT-New 2) and canonical PT marker gene LRP2. Note that some MYO5B expression is observed in control samples as expected from the CPM values presented in B. **B** Feature plots highlighting the expression of NQO1 and MYO5B in PTs (compare to Fig. 4A) as well as box plots showing the expression of the respective gene in PTs in control versus AKI samples. **C** *In situ* hybridizations for inflammation response gene SERPINA1 (marker gene for PT-New 3), EMT-associated gene VCAM1 (marker gene for PT-New 4), and canonical PT marker gene LRP2. Scale bars as indicated. P-value: * < 0.05, ** < 0.01, *** < 0.001. CPM, counts per million

**Fig. 5** (See legend on previous page.)

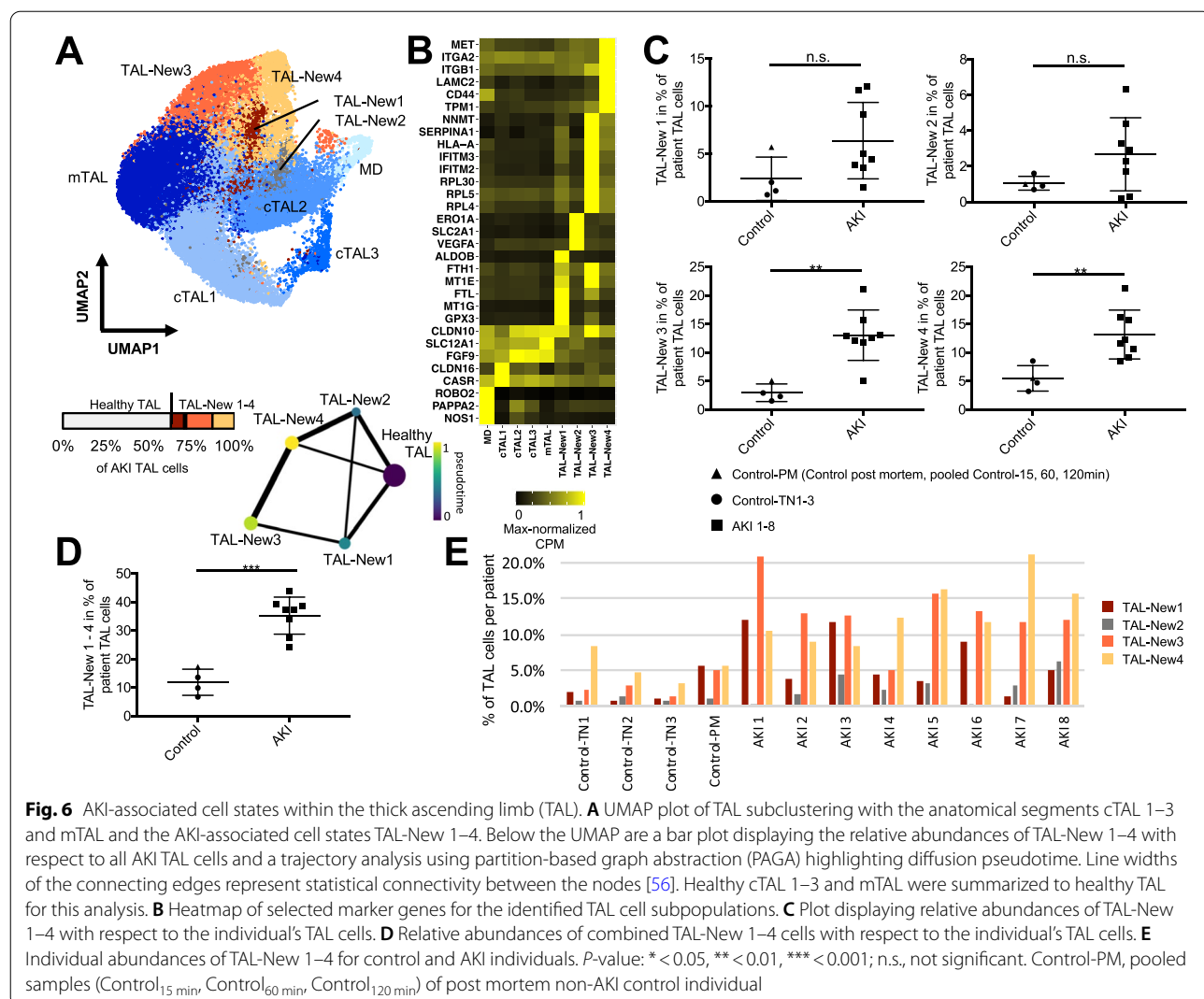


Fig. 6 AKI-associated cell states within the thick ascending limb (TAL). **A** UMAP plot of TAL subclustering with the anatomical segments cTAL 1–3 and mTAL and the AKI-associated cell states TAL-New 1–4. Below the UMAP are a bar plot displaying the relative abundances of TAL-New 1–4 with respect to all AKI TAL cells and a trajectory analysis using partition-based graph abstraction (PAGA) highlighting diffusion pseudotime. Line widths of the connecting edges represent statistical connectivity between the nodes [56]. Healthy cTAL 1–3 and mTAL were summarized to healthy TAL for this analysis. **B** Heatmap of selected marker genes for the identified TAL cell subpopulations. **C** Plot displaying relative abundances of TAL-New 1–4 with respect to the individual's TAL cells. **D** Relative abundances of combined TAL-New 1–4 cells with respect to the individual's TAL cells. **E** Individual abundances of TAL-New 1–4 for control and AKI individuals. *P*-value: * <0.05 , ** <0.01 , *** <0.001 ; n.s., not significant. Control-PM, pooled samples (Control_{15 min}, Control_{60 min}, Control_{120 min}) of post mortem non-AKI control individual

might be specific to AKI in the settings of critical illness and/or systemic inflammation.

Moreover, we used multi-channel RNAscope in situ hybridizations with probes against TAL-New 1–4 marker genes (Fig. 6B), again combining them with a canonical TAL marker gene encoding solute carrier family 12 member 1 (SLC12A1). We utilized marker transcripts for TAL-New 1 (oxidative stress signature, marker gene: aldolase B, ALDOB), TAL-New 2 (hypoxia signature; marker gene: solute carrier family 2 member 1, SLC2A1), TAL-New 3 (inflammation response signature; marker gene: serpin family A member 1, SERPINA1), and TAL-New 4 (EMT signature; marker gene: MET proto-oncogene, MET) [60, 63–65]. Similar to our findings in proximal tubules, TAL-New 1–4 cell states were confirmed to represent distinct cells that were interspersed within the TAL of AKI patients (Fig. 7A–D).

Similar to the PT, we also observed inter-individual heterogeneity for the AKI-associated cell states in other

cell types of the kidney tubule (Fig. 6E, Additional file 1: Fig. S10–12). Although, similar clusters as PT-New 1–4 were present in the other kidney tubule cell types, their relative abundance was cell type-dependent. In PTs and DCTs, the most abundant AKI-associated cell state was that associated with EMT (PT-New 4 and DCT-New 4). In contrast, the most abundant TAL cell state was TAL-New 3 (interferon gamma signaling-associated). We conclude that injury responses in different epithelial cell types of the kidney associate with common molecular pathways and marker genes, although they display cell type-specific and inter-individual heterogeneity.

Discussion

This study identifies a strong impact of human AKI associated with critical illness on the kidney transcriptome at single cell resolution. We provide an atlas of single cell transcriptomes and uncover novel AKI-induced transcriptomic responses at unprecedented cellular

resolution and transcriptional depth. We find that the dominant AKI-associated transcriptomic alterations reside within the different cell types of the kidney's tubular epithelium with surprisingly few transcriptomic alterations in other cell types. We uncover four AKI-associated "New" transcriptomic cell states, which emerge abundantly in PT, TAL, and DCT and display a remarkable overlap of marker genes and enriched molecular pathways between these different tubular epithelial cell types, suggesting common injury mechanisms. We were able to validate all four cell states in PTs and TALs using multi-channel *in situ* hybridization. Finally, we report a strong transcriptional heterogeneity among individuals with AKI, which is explained by the inter-individual differences in cell type-specific abundances of injury-associated cell states.

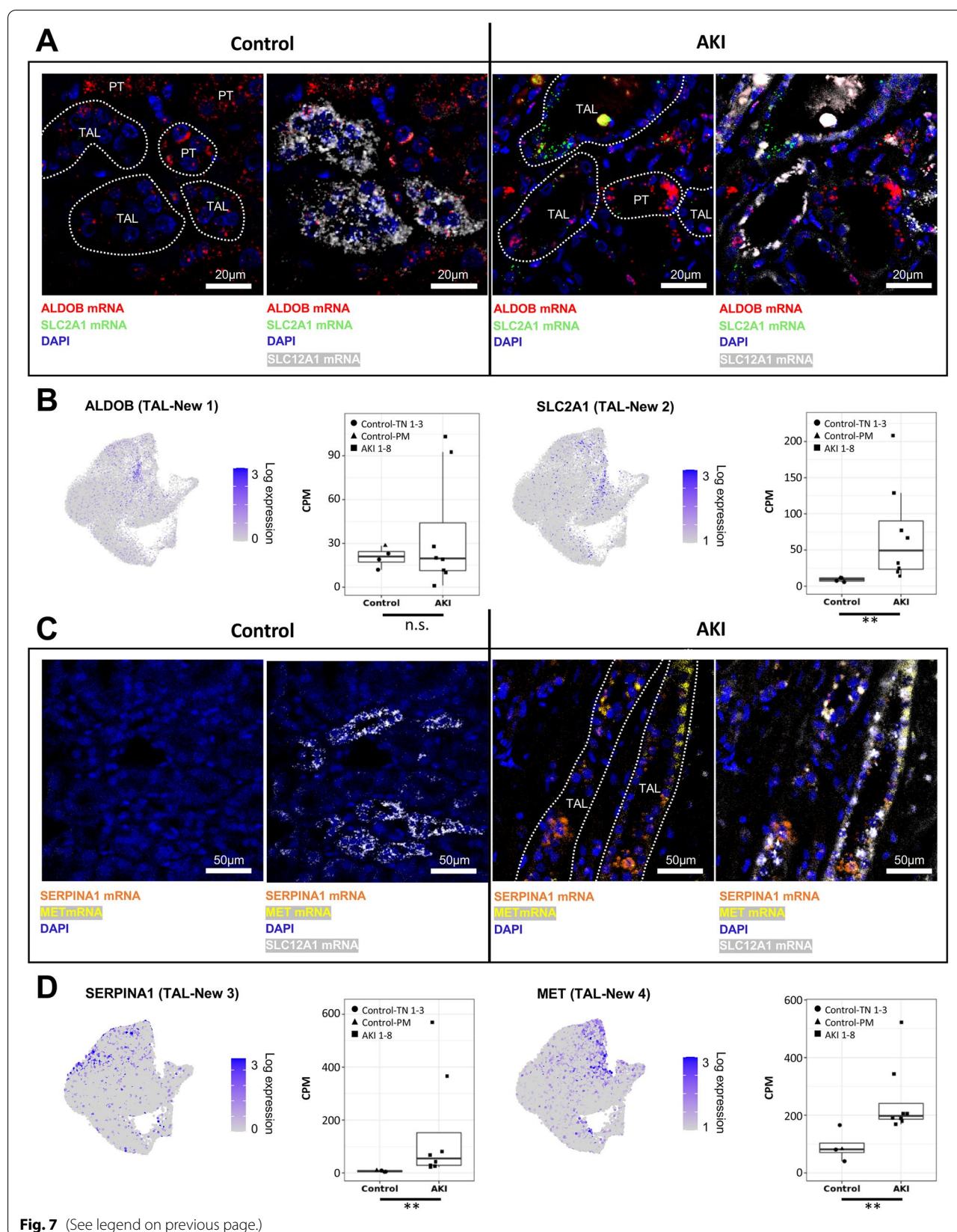
Our study provides insights into the pathophysiology of human AKI and indicates injury-associated responses in several different types of tubular epithelial cells. Previous studies of AKI in animal models (mostly ischemia–reperfusion injury in mice) have focused on the PT because cells of the PT are abundant and because PTs display marked susceptibility and responsiveness to ischemic injury [13, 14, 44, 45, 66–68]. Fewer studies have examined effects of AKI on other cell types. However, some previous rodent studies also showed evidence of injury in distal parts of the kidney tubule including TALs [69] and collecting ducts [70], similar to what we demonstrate here in human AKI. Presumed mechanisms of tubular injury and tubular transcriptome responses are related to the high metabolic demands of tubular cells, in particular PTs and TALs, which become overwhelmed in the setting of ischemia or hypoxia [44, 69, 71, 72]. Tubular stress in this setting is documented by novel induction of injury-associated transcripts and downregulation of differentiation markers (e.g., solute transporters). Most recently, transcriptome studies at single cell resolution in mouse AKI models confirmed these findings and indicated predominant cellular responses in the proximal tubule compartment of the kidney [11, 12, 30]. Our human AKI data are consistent with the proximal tubular responses described in mice, but they suggest an unexpectedly widespread molecular response in other types of kidney tubular epithelia, including TAL, DCT, CNT, and

collecting duct. It is tempting to assume that this difference reflects the more complex, multifactorial pathogenesis of AKI in critically ill patients compared to ischemia reperfusion models, but additional interspecies differences can so far not be excluded. Moreover, in the PT, the chronological order of appearance of the injured clusters seems to be different from mice (e.g., presence of injured PT-S1/2, PT-S3 and failed repair cells at the same time) [11]. This might highlight different molecular processes in humans when compared to mice or might be due to a setting of constant ongoing injury in humans in contrast to experimentally induced renal injury at a single defined time point in mouse models.

Given the observed induction of AKI-associated cell states in different segments of the kidney tubule, questions arise regarding their functional significance. It is noteworthy that we found a particularly pronounced activation of NRF2 target genes in the "New 1" clusters in several cell types (PT-New 1, TAL-New 1, DCT-New 1, CNT-New 1, CD-PC-New 1, TL-New 1). NRF2 signaling is induced by oxidative stress, plays a role in the induction of antioxidative genes, and has been associated with protection from kidney injury [73–75]. Trajectory analyses and comparative genomics indicated that these cells were likely derived from S1/2 segments of the PT and represent an early stage of injury. Cells of the "New 2" cluster exhibited a hypoxia signature. Hypoxia has also previously been recognized as an important mechanism of AKI, due to low baseline tissue oxygen concentrations in the kidney, which further decline under conditions leading to AKI. Induction of hypoxia-inducible genes through stabilization of hypoxia-inducible transcription factors in different kidney cell populations or selectively in TAL or PT cells was found to ameliorate ischemic or toxic AKI [45, 76]. In contrast, cells of the "New 3" and "New 4" clusters expressed an EMT signature and pro-inflammatory genes and resembled cells previously described as a "failed repair" state, which is associated with progression to kidney fibrosis [11, 57]. In trajectory analyses, these cells were transcriptionally most distant from healthy tubular epithelium in PT and TAL. Our study provides evidence for patient-specific individual compositions of AKI-associated cell states, but it does not support an existence of strictly different molecular

(See figure on next page.)

Fig. 7 Multi-channel *in situ* hybridizations confirm the presence of the four "New" cell states in TALs. **A** *In situ* hybridizations for oxidative stress-related gene ALDOB (marker gene of TAL-New 1), hypoxia-induced gene SLC2A1 (marker gene of TAL-New 2), and canonical TAL marker gene SLC12A1. Note that the TAL-New 1 abundance is not significantly different between AKI and control samples (compare to Fig. 6B). TAL-New 1 cells based on ALDOB expression are therefore also present in control samples. Moreover, ALDOB is also expressed in PT cells. **B** Feature plots highlighting the expression of ALDOB and SLC2A1 in TALs (compare to Fig. 6A) as well as box plots showing the expression of the respective genes in TALs in control versus AKI samples. **C** *In situ* hybridizations for inflammation response gene SERPINA1 (marker gene of TAL-New 3), EMT-associated gene MET (marker gene of TAL-New 4), and canonical TAL marker gene SLC12A1. Scale bars as indicated. *P*-value: * <0.05 , ** <0.01 , *** <0.001 . CPM, counts per million

**Fig. 7** (See legend on previous page.)

subtypes of AKI. Nevertheless, larger cohorts will be needed to confirm this notion.

Our study included patients with COVID-19-associated AKI. There is an ongoing debate on the mechanisms of AKI in COVID-19, particularly with regard to whether there is a COVID-19-specific kidney pathophysiology that is different from other critical illness-associated forms of AKI [26, 28, 52, 77, 78]. Our study did not uncover a specific transcriptomic signature associated with COVID-19-associated AKI and suggests that COVID-19 AKI is on a common molecular spectrum with AKI associated with other types of respiratory failure and critical illness. However, future studies with increased patient numbers and functional studies are required to provide definitive answers in this regard.

In summary, we observed that AKI in humans with critical illness and systemic inflammation is associated with widespread transcriptomic responses within a spectrum of kidney cell types, uncovering novel cell states and potential targets for AKI therapies. These findings suggest that precision approaches like single-cell transcriptomics may be suitable tools to overcome the current limitations in diagnosing and treating subtypes of AKI.

Conclusions

Single-cell transcriptomics revealed recurring AKI-associated epithelial cell states throughout the cell types of the kidney tubular epithelium. Our observation of patient-specific heterogeneity of these responses underlines the potential utility of single-cell approaches in informing personalized AKI management.

Supplementary Information

The online version contains supplementary material available at <https://doi.org/10.1186/s13073-022-01108-9>.

Additional file 1: **Fig. S1.** Basic statistics of snRNA-seq libraries. **Fig. S2.** PCA analyses of different cell types and whole tissue. **Fig. S3.** *In situ* staining for IGFBP7. **Fig. S4.** Number of differentially expressed genes between COVID AKI and non-COVID AKI. **Fig. S5.** Subclustering of leukocytes. **Fig. S6.** Abundances and marker genes from subclusterings of major cell types. **Fig. S7.** QC metrics for all subclusters. **Fig. S8.** Cluster abundances per cell type and sample. **Fig. S9.** Results from cross-species approach for human PT cells. **Fig. S10–12.** Subclusterings of remaining kidney epithelial cell types. **Fig. S13.** Joint heatmap for marker genes of the “New” clusters. **Fig. S14.** Validation of “New” clusters in PT and TAL cells in an independent dataset.

Additional file 2: **Table S1.** Clinical and histopathological information on included individuals.

Additional file 3: **Table S2.** Results from differential gene expression analysis control versus AKI.

Additional file 4: **Table S3.** Results from pathway enrichment analyses AKI versus controls.

Additional file 5: **Table S4.** Results from differential gene expression analysis COVID vs. non-COVID AKI.

Additional file 6: **Table S5.** Results from pathway enrichment analyses COVID AKI versus non-COVID AKI.

Additional file 7: **Table S6.** Marker genes of all identified sub cell types and cell states.

Additional file 8: **Table S7.** Marker gene comparison between AKI-induced cell states of PT, TAL and DCT.

Additional file 9: **Table S8.** Results from transcriptional regulation analysis on the joint marker genes of the New 1-4 cell states.

Acknowledgements

We thank Tatjana Luganskaja for excellent technical support. We thank Benjamin D. Humphreys and his lab for providing supplemental information to their original publication [11].

Authors' contributions

C.H., P.E., K.-U.E., N.R., C.K., and K.M.S.-O. designed the study and wrote the paper. C.H., C.K., C.H., and A.B. performed the single-nuclei sequencing experiments. J.L., S.C., and C.H. performed the bulk RNA sequencing and *in situ* hybridizations. Data was analyzed by C.H., N.K., C.K., C.M.S., J.K., B.O., L.H., E.W., M.L., N.H., and M.B. Analysis and assessment of clinical data were performed by C.H., J.H.H., H.S., and I.G. Histopathological analyses were conducted by S.B., A.H., W.S., and V.C. All authors read and approved the final manuscript.

Funding

This work was supported by grants to KMSO from the Deutsche Forschungsgemeinschaft (DFG; SFB 1365, GRK 2318 and FOR 2841), to C.H. from the DFG (HI 2238/2-1) and the Berlin Institute of Health (BIH) and MDC (BIH and MDC Focus Area Translational Vascular Biomedicine), and by the Urological Research Foundation (Berlin). ACH was supported by the Berlin University Alliance GC2 Global Health (Corona Virus Pre-Exploration Project), the BMBF (RAPID and Organo-Strat 01KX2021), and the DFG (SFB-TR 84, B6 / Z1a). PE was supported by DFG grant EN 924/5-1, the BIH, and the Jackstädt Foundation. NK was supported by DFG grants RA 838/5-1 and KA 5006/1-1. AB was supported by funding from the Gottfried Wilhelm Leibniz Prize of the DFG or NR.

Availability of data and materials

Single cell data can be accessed via: <https://shiny.mdc-berlin.de/humAKI>. Unfiltered Cellranger output files from all samples as well as meta data with cell type assignment can be downloaded at NCBI GEO under the accession number GSE210622.

Declarations

Ethics approval and consent to participate

Our study protocol was approved by Charité’s Ethics Committee (ethics approvals EA2/045/18 for post mortem kidney biopsies and EA4/026/18 for tumor-adjacent normal tissue) and was conducted by following the Declaration of Helsinki and Guidelines for Good Clinical Practice. Written informed consent was given by the next of kin before enrollment in our study.

Consent for publication

Not applicable.

Competing interests

The authors declare no competing interests.

Author details

¹Department of Nephrology and Hypertension, Hannover Medical School, Hannover, Germany. ²Department of Nephrology and Medical Intensive Care, Charité-Universitätsmedizin Berlin, Corporate Member of Freie Universität Berlin and Humboldt-Universität Zu Berlin, Berlin, Germany. ³Max Delbrück Center for Molecular Medicine in the Helmholtz Association, Berlin, Germany. ⁴Berlin Institute for Medical Systems Biology, Max Delbrück Center in the Helmholtz Association, Berlin, Germany. ⁵Deutsches RheumaForschungszentrum, an Institute of the Leibniz Foundation, Berlin, Germany. ⁶Berlin Institute of Health, Berlin, Germany. ⁷Core Unit Bioinformatics, BIH/Charité/MDC, Berlin, Germany.

⁸Institute for Functional Anatomy, Charité-Universitätsmedizin Berlin, Corporate Member of Freie Universität Berlin and Humboldt-Universität Zu Berlin, Berlin, Germany. ⁹Department of Infectious Diseases and Respiratory Medicine, Charité-Universitätsmedizin Berlin, Corporate Member of Freie Universität Berlin and Humboldt-Universität Zu Berlin, Berlin, Germany. ¹⁰Institute of Virology, Charité-Universitätsmedizin Berlin, Corporate Member of Freie Universität Berlin and Humboldt-Universität Zu Berlin, Berlin, Germany. ¹¹Department of Urology, Charité-Universitätsmedizin Berlin, Corporate Member of Freie Universität Berlin and Humboldt-Universität Zu Berlin, Berlin, Germany. ¹²Department of Pathology, Charité-Universitätsmedizin Berlin, Corporate Member of Freie Universität Berlin and Humboldt-Universität Zu Berlin, Berlin, Germany. ¹³Institute of Physiology, Christian-Albrechts-Universität, Kiel, Germany.

Received: 11 January 2022 Accepted: 12 August 2022

Published online: 09 September 2022

References

- Lafrance JP, Miller DR. Acute kidney injury associates with increased long-term mortality. *J Am Soc Nephrol*. 2010;21:345–52.
- Wang HE, Muntner P, Chertow GM, Warnock DG. Acute kidney injury and mortality in hospitalized patients. *Am J Nephrol*. 2012;35:349–55.
- Sawhney S, et al. Intermediate and long-term outcomes of survivors of acute kidney injury episodes: a large population-based cohort study. *Am J Kidney Dis*. 2017;69:18–28.
- Chertow GM, Burdick E, Honour M, Bonventre JV, Bates DW. Acute kidney injury, mortality, length of stay, and costs in hospitalized patients. *J Am Soc Nephrol*. 2005;16:3365–70.
- Chertow GM, et al. Mortality after acute renal failure: models for prognostic stratification and risk adjustment. *Kidney Int*. 2006;70:1120–6.
- Liangos O, et al. Epidemiology and outcomes of acute renal failure in hospitalized patients: a national survey. *Clin J Am Soc Nephrol*. 2006;1:43–51.
- Uchino S, et al. Acute renal failure in critically ill patients: a multinational, multicenter study. *JAMA*. 2005;294:813–8.
- Chen H, Busse LW. Novel therapies for acute kidney injury. *Kidney Int Rep*. 2017;2:785–99.
- Moore PK, Hsu RK, Liu KD. Management of acute kidney injury: Core Curriculum 2018. *Am J Kidney Dis*. 2018;72:136–48.
- Prowle JR, Bellomo R. Continuous renal replacement therapy: recent advances and future research. *Nat Rev Nephrol*. 2010;6:521–9.
- Kirita Y, Wu H, Uchimura K, Wilson PC, Humphreys BD. Cell profiling of mouse acute kidney injury reveals conserved cellular responses to injury. *Proc Natl Acad Sci U S A*. 2020;117:15874–83.
- Rudman-Melnick V, et al. Single-Cell Profiling of AKI in a murine model reveals novel transcriptional signatures, profibrotic phenotype, and epithelial-to-stromal crosstalk. *J Am Soc Nephrol*. 2020;31:2793–814.
- Marko L, et al. Tubular epithelial NF-κappaB activity regulates ischemic AKI. *J Am Soc Nephrol*. 2016;27:2658–69.
- Vigolo E, et al. Canonical BMP signaling in tubular cells mediates recovery after acute kidney injury. *Kidney Int*. 2019;95:108–22.
- Xu K, et al. Unique transcriptional programs identify subtypes of AKI. *J Am Soc Nephrol*. 2017;28:1729–40.
- Zhang WR, Parikh CR. Biomarkers of acute and chronic kidney disease. *Annu Rev Physiol*. 2019;81:309–33.
- Menez S, et al. Urinary EGF and MCP-1 and risk of CKD after cardiac surgery. *JCI Insight*. 2021;6:e147464.
- de Boer IH, et al. Rationale and design of the Kidney Precision Medicine Project. *Kidney Int*. 2021;99:498–510.
- Bhatraju PK, et al. Acute kidney injury subphenotypes based on creatinine trajectory identifies patients at increased risk of death. *Crit Care*. 2016;20:372.
- Kellum JA, Sileanu FE, Bihorac A, Hoste EA, Chawla LS. Recovery after acute kidney injury. *Am J Respir Crit Care Med*. 2017;195:784–91.
- Hardenberg JB, et al. Critical illness and systemic inflammation are key risk factors of severe acute kidney injury in patients with COVID-19. *Kidney Int Rep*. 2021;6:905–15.
- Hirsch JS, et al. Acute kidney injury in patients hospitalized with COVID-19. *Kidney Int*. 2020;98:209–18.
- Cummings MJ, et al. Epidemiology, clinical course, and outcomes of critically ill adults with COVID-19 in New York City: a prospective cohort study. *Lancet*. 2020;395:1763–70.
- Gabarre P, et al. Acute kidney injury in critically ill patients with COVID-19. *Intensive Care Med*. 2020;46:1339–48.
- Werion A, et al. SARS-CoV-2 causes a specific dysfunction of the kidney proximal tubule. *Kidney Int*. 2020;98:1296–307.
- Braun F, et al. SARS-CoV-2 renal tropism associates with acute kidney injury. *Lancet*. 2020;396:597–8.
- Kudose S, et al. Kidney biopsy findings in patients with COVID-19. *J Am Soc Nephrol*. 2020;31:1959–68.
- Sharma P, et al. COVID-19-Associated kidney injury: a case series of kidney biopsy Findings. *J Am Soc Nephrol*. 2020;31:1948–58.
- Xia P, et al. Clinicopathological features and outcomes of acute kidney injury in critically ill COVID-19 with prolonged disease course: a retrospective cohort. *J Am Soc Nephrol*. 2020;31:2205–21.
- Gerhardt LMS, Liu J, Koppitch K, Cippa PE, McMahon AP. Single-nuclear transcriptomics reveals diversity of proximal tubule cell states in a dynamic response to acute kidney injury. *Proc Natl Acad Sci U S A*. 2021;118:e2026684118.
- Leiz J, et al. Nuclei isolation from adult mouse kidney for single-nucleus RNA-sequencing. *J Vis Exp*. 2021;20:e62901.
- Dobin A, et al. STAR: ultrafast universal RNA-seq aligner. *Bioinformatics*. 2013;29:15–21.
- Liao Y, Smyth GK, Shi W. featureCounts: an efficient general purpose program for assigning sequence reads to genomic features. *Bioinformatics*. 2014;30:923–30.
- Love MI, Huber W, Anders S. Moderated estimation of fold change and dispersion for RNA-seq data with DESeq2. *Genome Biol*. 2014;15:550.
- Subramanian A, et al. Gene set enrichment analysis: a knowledge-based approach for interpreting genome-wide expression profiles. *Proc Natl Acad Sci U S A*. 2005;102:15545–50.
- Liberzon A, et al. Molecular signatures database (MSigDB) 3.0. *Bioinformatics*. 2011;27:1739–40.
- Nishimura D. BioCarta. *Biotech Softw Internet Rep*. 2001;2:117–20.
- Ogata H, et al. KEGG: Kyoto Encyclopedia of Genes and Genomes. *Nucleic Acids Res*. 1999;27:29–34.
- Gillespie M, et al. The reactome pathway knowledgebase 2022. *Nucleic Acids Res*. 2022;50:D687–92.
- Slenter DN, et al. WikiPathways: a multifaceted pathway database bridging metabolomics to other omics research. *Nucleic Acids Res*. 2018;46:D661–7.
- Wolf FA, Angerer P, Theis FJ. SCANPY: large-scale single-cell gene expression data analysis. *Genome Biol*. 2018;19:15.
- Friedman J, Hastie T, Tibshirani R. Regularization paths for generalized linear models via coordinate descent. *J Stat Softw*. 2010;33:1–22.
- Lake B.B., et al. An atlas of healthy and injured cell states and niches in the human kidney. *bioRxiv*, 2021; 2021.2007.2028.454201. <https://doi.org/10.1101/2021.07.28.454201>.
- Heyman SN, Rosenberger C, Rosen S. Experimental ischemia-reperfusion: biases and myths—the proximal vs. distal hypoxic tubular injury debate revisited. *Kidney Int*. 2010;77:9–16.
- Scholz H, et al. Kidney physiology and susceptibility to acute kidney injury: implications for renoprotection. *Nat Rev Nephrol*. 2021;17:335–49.
- Sriswat N, Kellum JA. The role of biomarkers in acute kidney injury. *Crit Care Clin*. 2020;36:125–40.
- Paragas N, et al. The Ngf reporter mouse detects the response of the kidney to injury in real time. *Nat Med*. 2011;17:216–22.
- Ichimura T, et al. Kidney injury molecule-1 (KIM-1), a putative epithelial cell adhesion molecule containing a novel immunoglobulin domain, is up-regulated in renal cells after injury. *J Biol Chem*. 1998;273:4135–42.
- Cen C, et al. Osteopontin blockade attenuates renal injury after ischemia reperfusion by inhibiting NK cell infiltration. *Shock*. 2017;47:52–60.
- Emlet DR, et al. Insulin-like growth factor binding protein 7 and tissue inhibitor of metalloproteinases-2: differential expression and secretion in human kidney tubule cells. *Am J Physiol Renal Physiol*. 2017;312:F284–96.
- Gomez H, Kellum JA, Ronco C. Metabolic reprogramming and tolerance during sepsis-induced AKI. *Nat Rev Nephrol*. 2017;13:143–51.
- Jansen J, et al. SARS-CoV-2 infects the human kidney and drives fibrosis in kidney organoids. *Cell Stem Cell*. 2022;29:217–31 (e218).

53. Bouquegneau A, et al. COVID-19-associated nephropathy includes tubular necrosis and capillary congestion, with evidence of SARS-CoV-2 in the nephron. *Kidney360*. 2021;2:639–52.
54. Bonventre JV. Dedifferentiation and proliferation of surviving epithelial cells in acute renal failure. *J Am Soc Nephrol*. 2003;14(Suppl 1):S55–61.
55. Chen EY, et al. Enrichr: interactive and collaborative HTML5 gene list enrichment analysis tool. *BMC Bioinformatics*. 2013;14:128.
56. Wolf FA, et al. PAGA: graph abstraction reconciles clustering with trajectory inference through a topology preserving map of single cells. *Genome Biol*. 2019;20:59.
57. Muto Y, et al. Single cell transcriptional and chromatin accessibility profiling redefine cellular heterogeneity in the adult human kidney. *Nat Commun*. 2021;12:2190.
58. Ross D, Siegel D. The diverse functionality of NQO1 and its roles in redox control. *Redox Biol*. 2021;41:101950.
59. Pamenter ME, Hall JE, Tanabe Y, Simonson TS. Cross-species insights into genomic adaptations to hypoxia. *Front Genet*. 2020;11:743.
60. Sanders CL, Ponte A, Kueppers F. The effects of inflammation on alpha 1 antitrypsin levels in a national screening cohort. *COPD*. 2018;15:10–6.
61. Zhang D, et al. VCAM1 promotes tumor cell invasion and metastasis by inducing EMT and transendothelial migration in colorectal cancer. *Front Oncol*. 2020;10:1066.
62. Lachmann A, et al. ChEA: transcription factor regulation inferred from integrating genome-wide ChIP-X experiments. *Bioinformatics*. 2010;26:2438–44.
63. Wang J, Wu Q, Qiu J. Accumulation of fructose 1,6-bisphosphate protects clear cell renal cell carcinoma from oxidative stress. *Lab Invest*. 2019;99:898–908.
64. Zhang JZ, Behrooz A, Ismail-Beigi F. Regulation of glucose transport by hypoxia. *Am J Kidney Dis*. 1999;34:189–202.
65. Jeon HM, Lee J. MET: roles in epithelial-mesenchymal transition and cancer stemness. *Ann Transl Med*. 2017;5:5.
66. Heyman SN, Brezis M, Epstein FH, Spokes K, Rosen S. Effect of glycine and hypertrophy on renal outer medullary hypoxic injury in ischemia reflow and contrast nephropathy. *Am J Kidney Dis*. 1992;19:578–86.
67. Heyman SN, Brezis M, Greenfeld Z, Rosen S. Protective role of furosemide and saline in radiocontrast-induced acute renal failure in the rat. *Am J Kidney Dis*. 1989;14:377–85.
68. Ramesh G, Ranganathan P. Mouse models and methods for studying human disease, acute kidney injury (AKI). *Methods Mol Biol*. 2014;1194:421–36.
69. Heyman SN, Shina A, Brezis M, Rosen S. Proximal tubular injury attenuates outer medullary hypoxic damage: studies in perfused rat kidneys. *Exp Nephrol*. 2002;10:259–66.
70. Rosenberger C, et al. Acute kidney injury in the diabetic rat: studies in the isolated perfused and intact kidney. *Am J Nephrol*. 2008;28:831–9.
71. Brezis M, Rosen S. Hypoxia of the renal medulla—its implications for disease. *N Engl J Med*. 1995;332:647–55.
72. Heyman SN, Fuchs S, Brezis M. The role of medullary ischemia in acute renal failure. *New Horiz*. 1995;3:597–607.
73. Nezu M, Suzuki N, Yamamoto M. Targeting the KEAP1-NRF2 system to prevent kidney disease progression. *Am J Nephrol*. 2017;45:473–83.
74. Bartz RR, Piantadosi CA. Clinical review: oxygen as a signaling molecule. *Crit Care*. 2010;14:234.
75. Wei W, Ma N, Fan X, Yu Q, Ci X. The role of Nrf2 in acute kidney injury: Novel molecular mechanisms and therapeutic approaches. *Free Radic Biol Med*. 2020;158:1–12.
76. Schley G, et al. Hypoxia-inducible transcription factors stabilization in the thick ascending limb protects against ischemic acute kidney injury. *J Am Soc Nephrol*. 2011;22:2004–15.
77. Fisher M, et al. AKI in hospitalized patients with and without COVID-19: a comparison study. *J Am Soc Nephrol*. 2020;31:2145–57.
78. Ferlicot S, et al. The spectrum of kidney biopsies in hospitalized patients with COVID-19, acute kidney injury, and/or proteinuria. *Nephrol Dial Transplant*. 2021;36:1253–62.

Publisher's Note

Springer Nature remains neutral with regard to jurisdictional claims in published maps and institutional affiliations.

Ready to submit your research? Choose BMC and benefit from:

- fast, convenient online submission
- thorough peer review by experienced researchers in your field
- rapid publication on acceptance
- support for research data, including large and complex data types
- gold Open Access which fosters wider collaboration and increased citations
- maximum visibility for your research: over 100M website views per year

At BMC, research is always in progress.

Learn more biomedcentral.com/submissions

